Table I.

The average grain size of different laser energy density

(scan pitch fixed to 2um)

Laser	SSL					ELA
Laser energy density (mJ/cm^2)	392	415	438	461	507	380
Grain size (μm)	0.1	0.3	0.55	0.7	1	0.3

Table II

The trap density of ELA (380mJ/cm^2) and SSL with laser energy of 415mJ/cm^2 to 507mJ/cm^2

Laser energy density (mJ/cm^2)	415	438	461	507	ELA
Trap density ($10^{12}/cm^2$)	1.37	1.25	1.14	1.03	1.84

Chapter 1

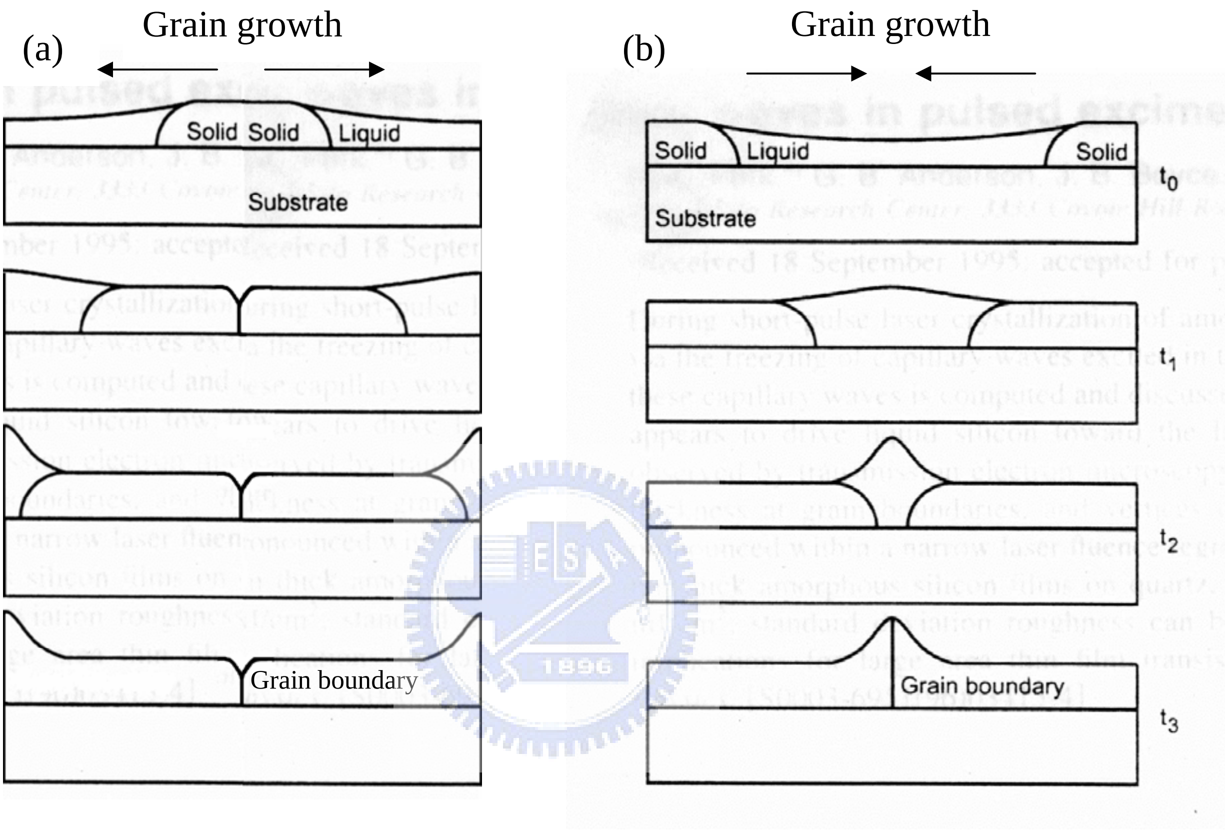

Fig.1-4-1 The simple schematic diagram of melted silicon (a) flow from the edge to the middle (b) flow from the middle to the edge during crystallization

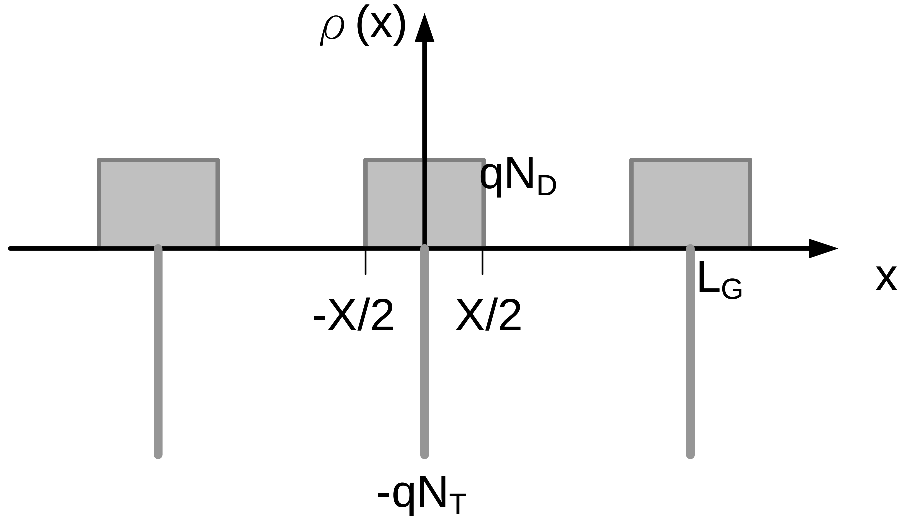

Fig.1-5-1 The distribution of the charges in poly-Si

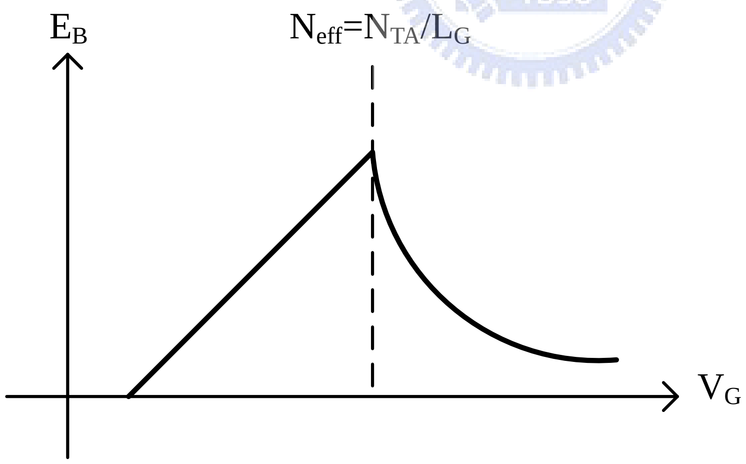

Fig.1-5-2 The relationship between energy barrier height and gate voltage

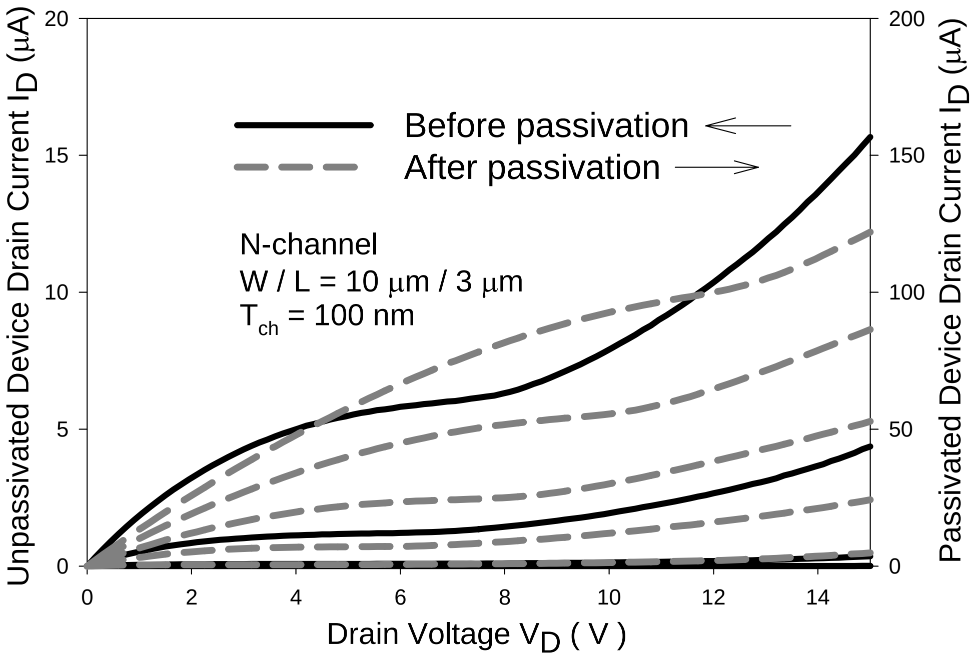

Fig.1-5-3 The output characteristic of device before and after passivation

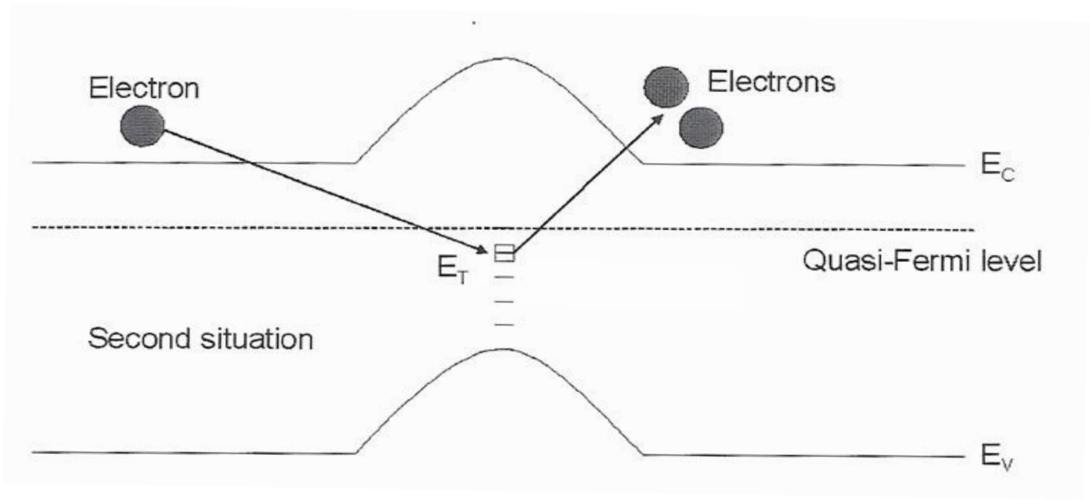

Fig.1-5-4 The "activation energy" is from this charged trap energy level to the conduction band edge

Chapter 2

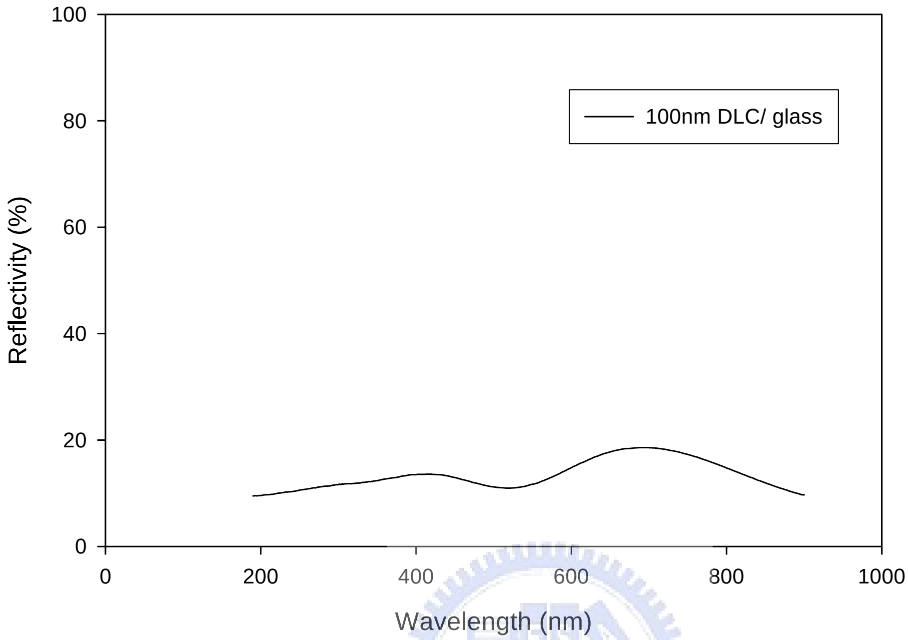

Fig.2-2-1 The reflectivity of DLC film. The thickness of DLC is 100*nm*

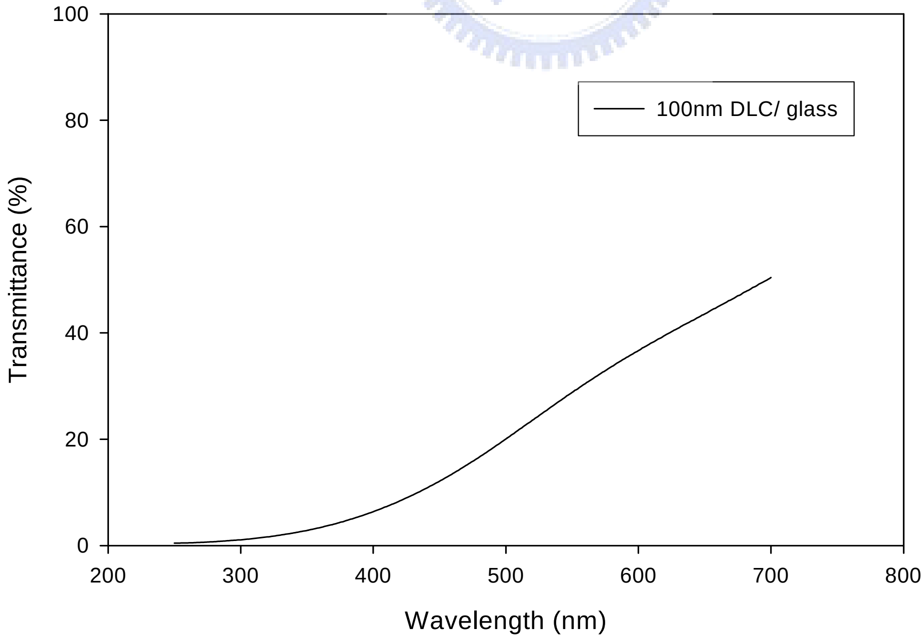

Fig.2-2-2 The transmittance of DLC film. The thickness of DLC is 100*nm*

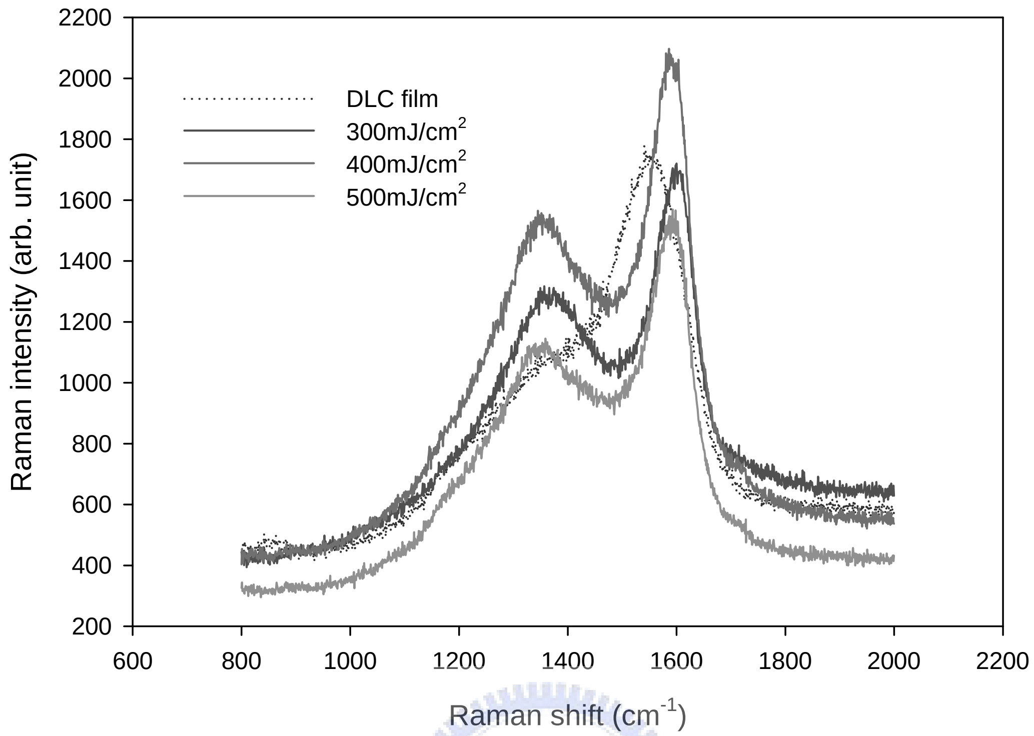

Fig.2-2-3 The Raman spectrum of DLC before and after laser irradiated by 300 to 500mJ/cm^2

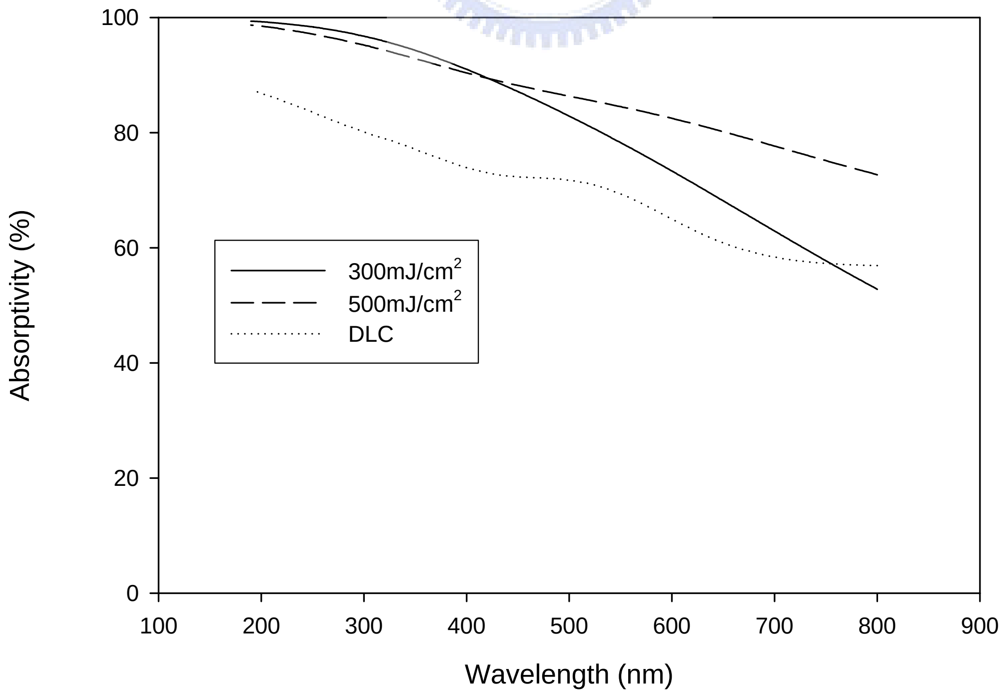

Fig.2-2-4 The calculated absorptivity of DLC films before and after laser irradiation with laser energy density of 300 and 500mJ/cm^2

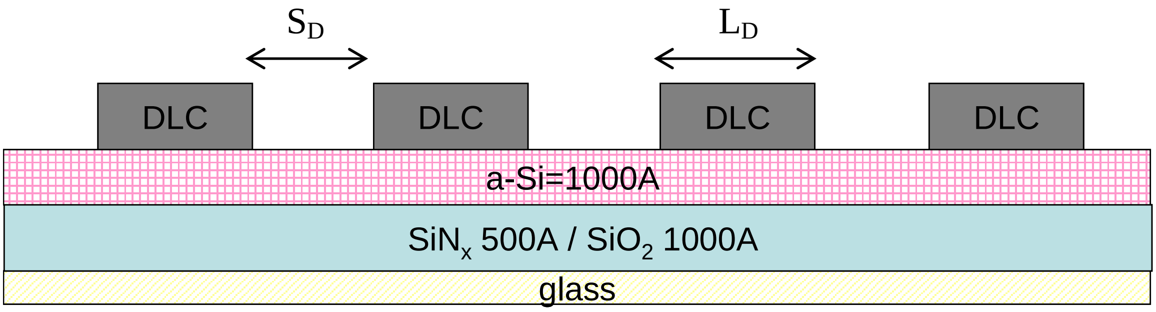

Fig.2-3-1 The cross-section of sample A. The space between DLC pattern are 3,6,10,20,30,50*um* and the length of DLC are 4,6,8,12,16,20,30,60*um*

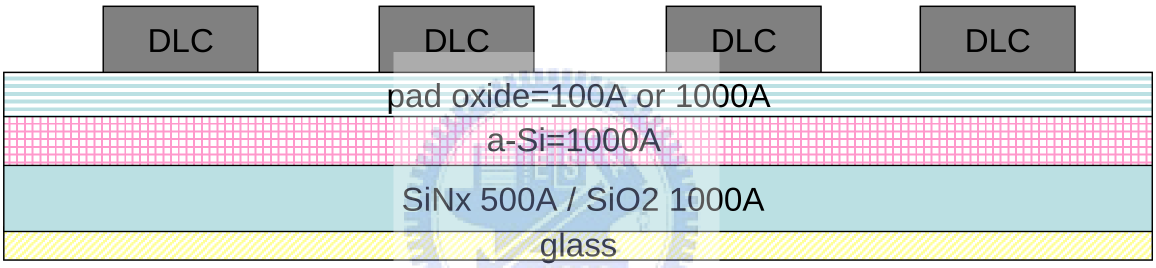

Fig.2-3-2(a) The cross-section of sample B

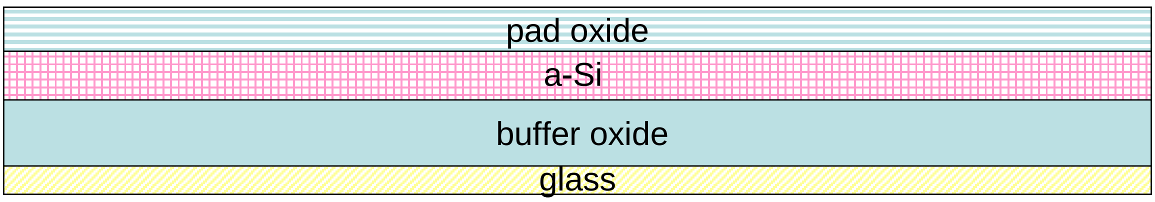

Fig.2-3-2(b) The cross-section of reference of sample B

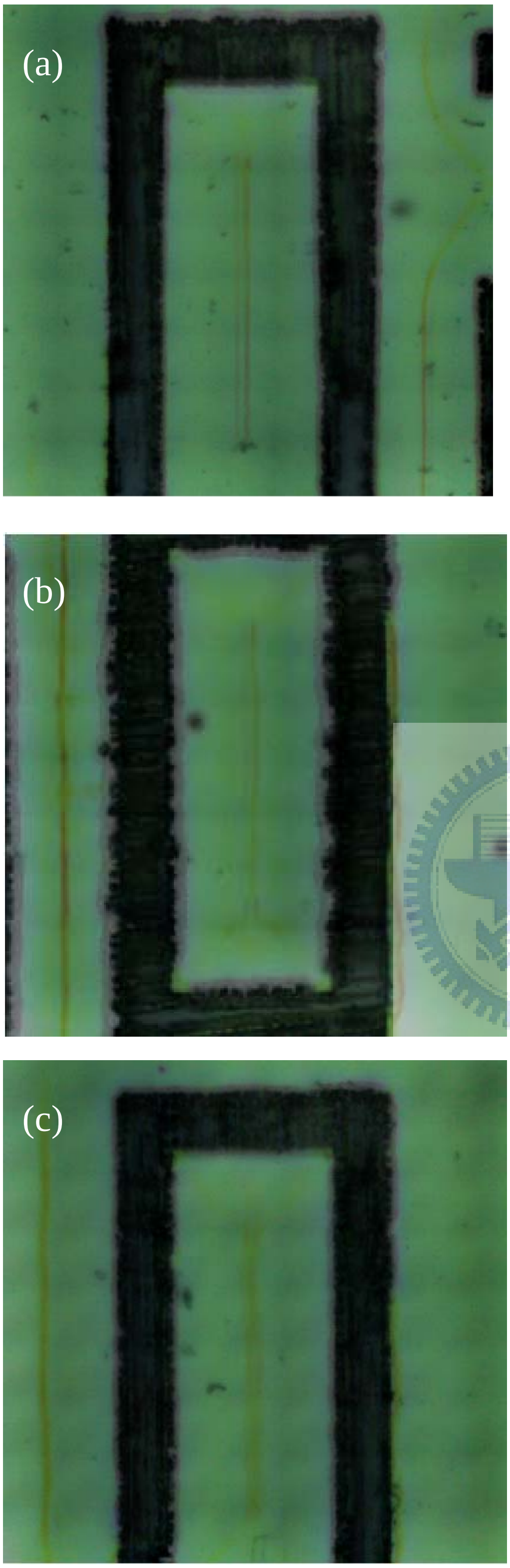

Fig.2-3-3 The OM image of sample A with the laser energy density of (a) 400mJ/cm^2 (b) 500mJ/cm^2 (c) 600mJ/cm^2

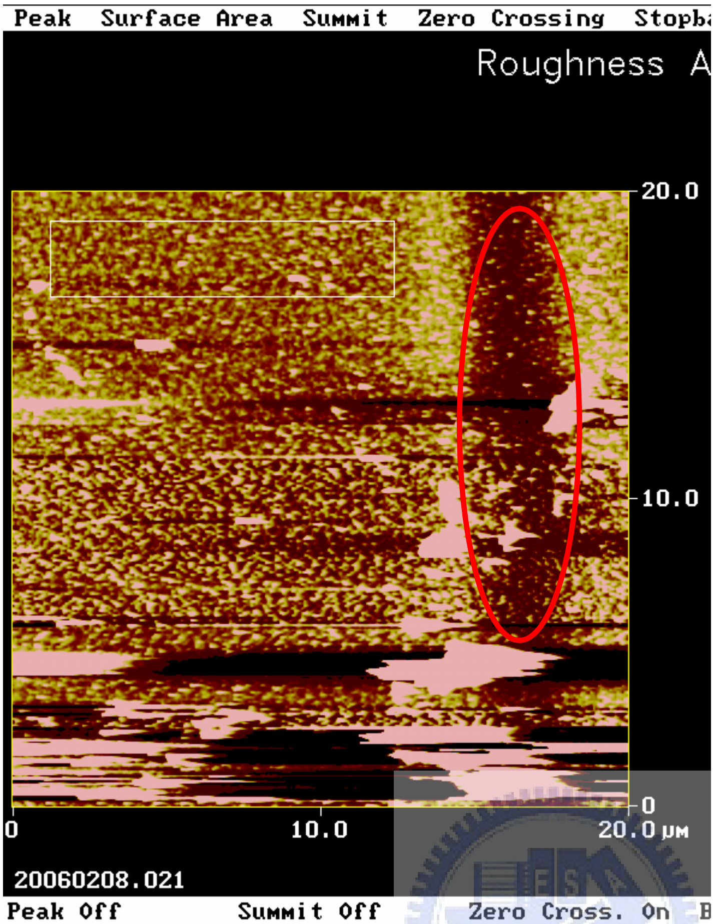

Fig.2-3-4 The AFM result of the region near the middle of the DLC patterns

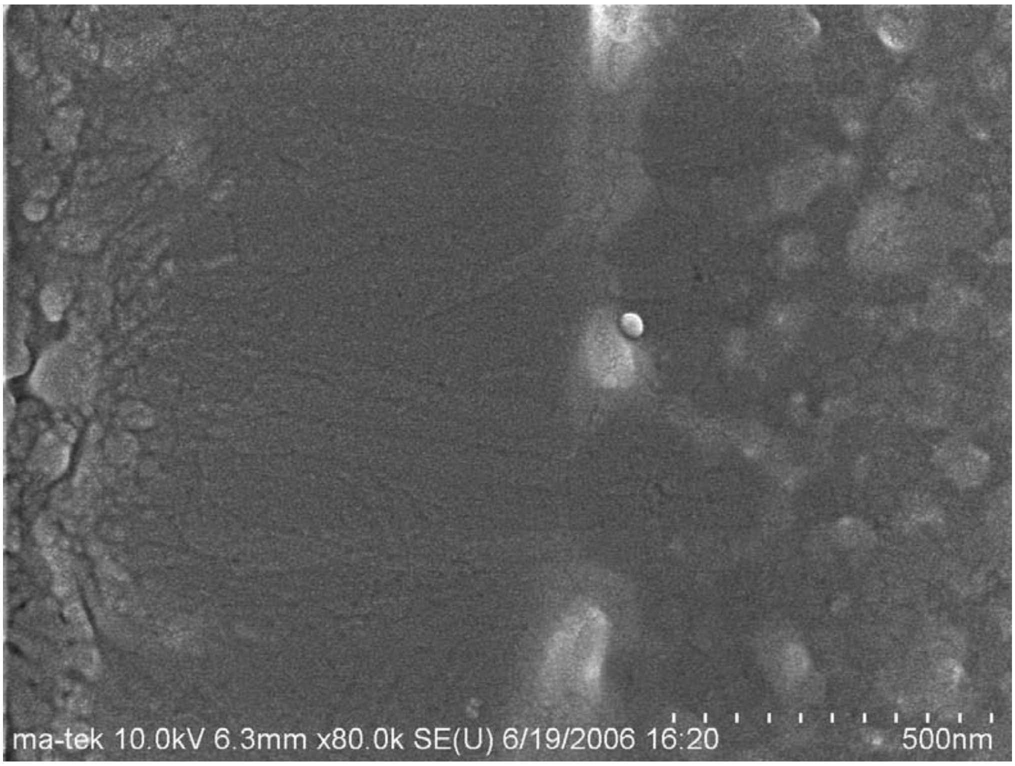

Fig.2-3-5 (a) SEM image of sample A with laser energy density of 400*mJ/cm*^{2}

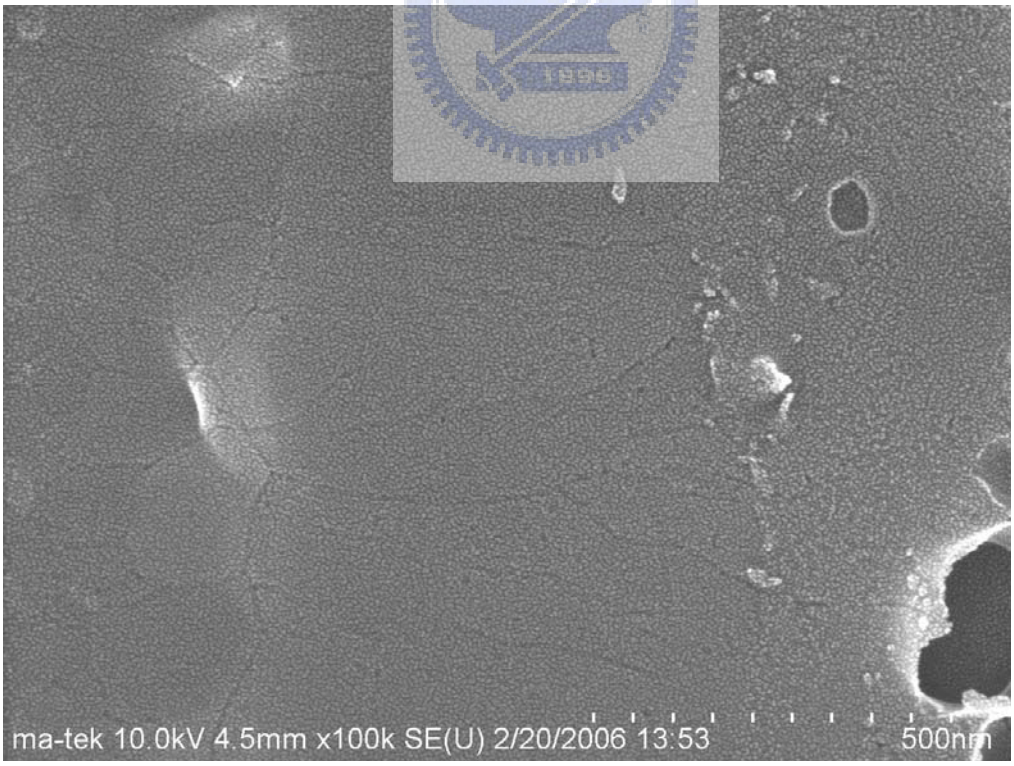

Fig. 2-3-5 (b) SEM image of sample A with laser energy density of 500*mJ/cm*^{2}

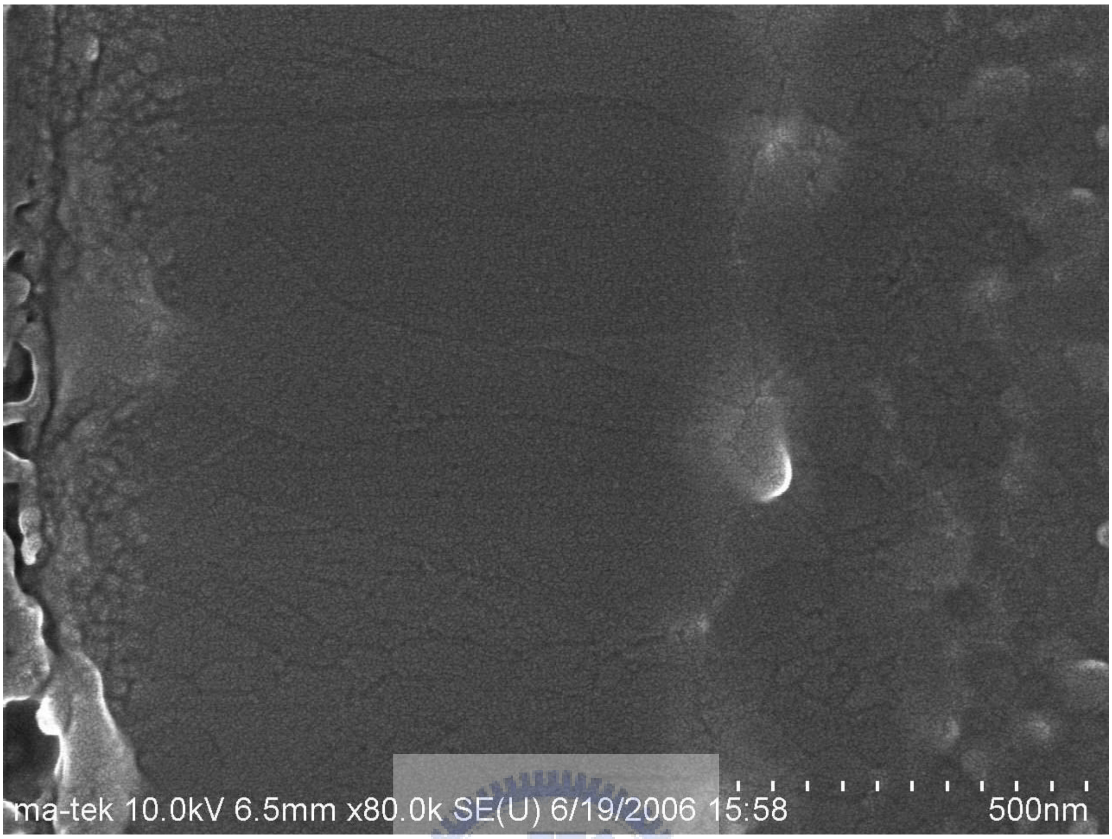

Fig. 2-3-5 (c) SEM image of sample A with laser energy density of 600mJ/cm^2

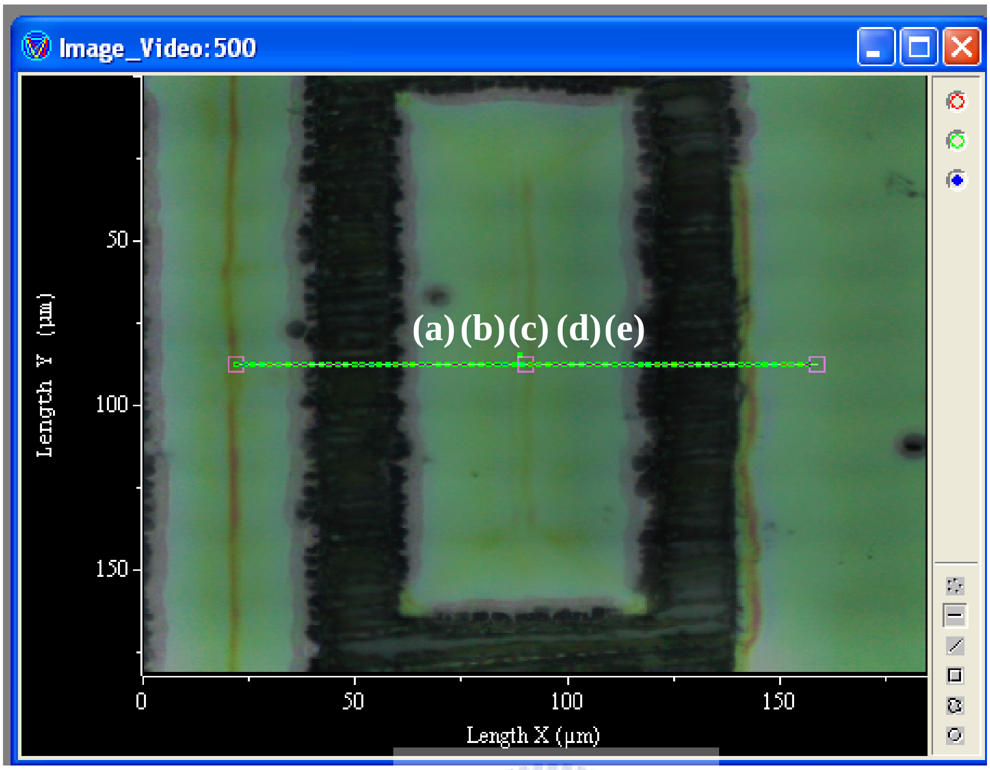

Fig.2-3-6 (a) The position of Raman irradiated

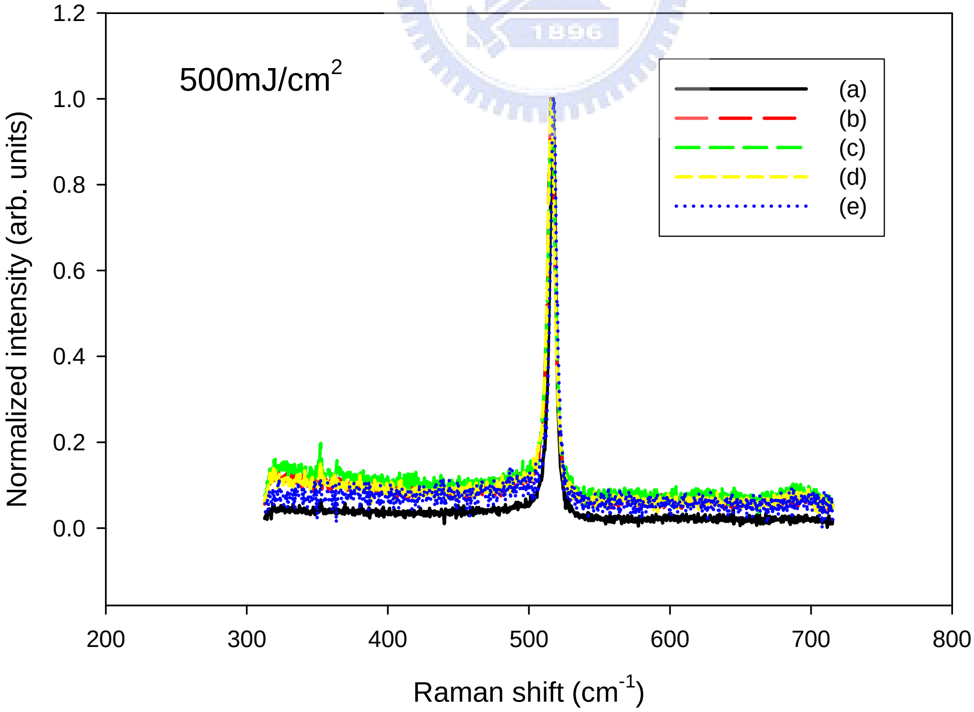

Fig. 2-3-6 (b) The Raman spectra of different position which is shown as Fig. 2-3-6(a)

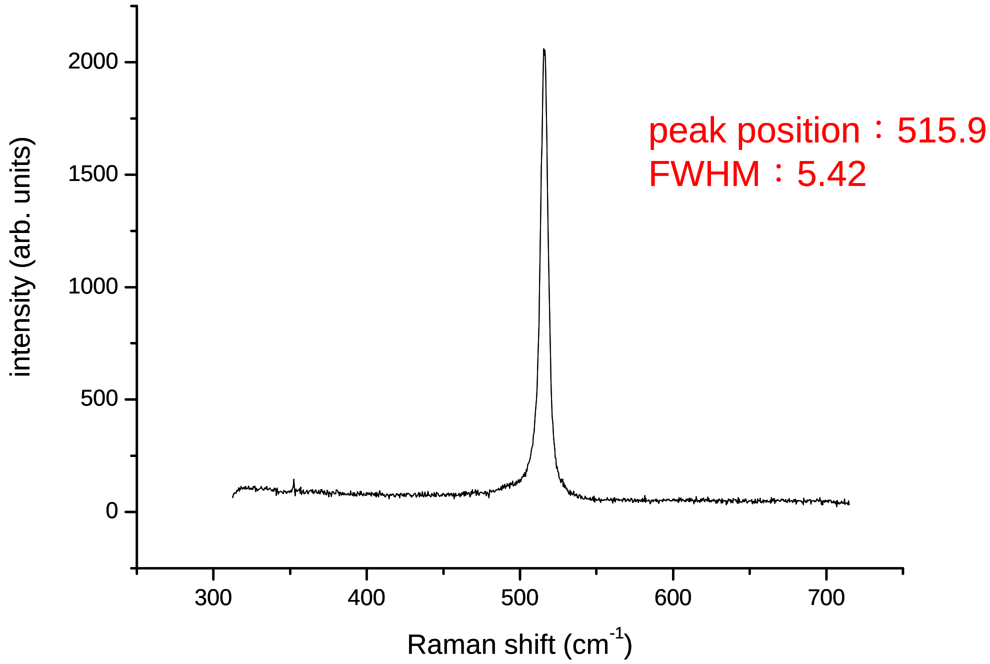

Fig.2-3-7(a) The Raman result of sample A with the laser energy density of 400*mJ/cm*^{2}

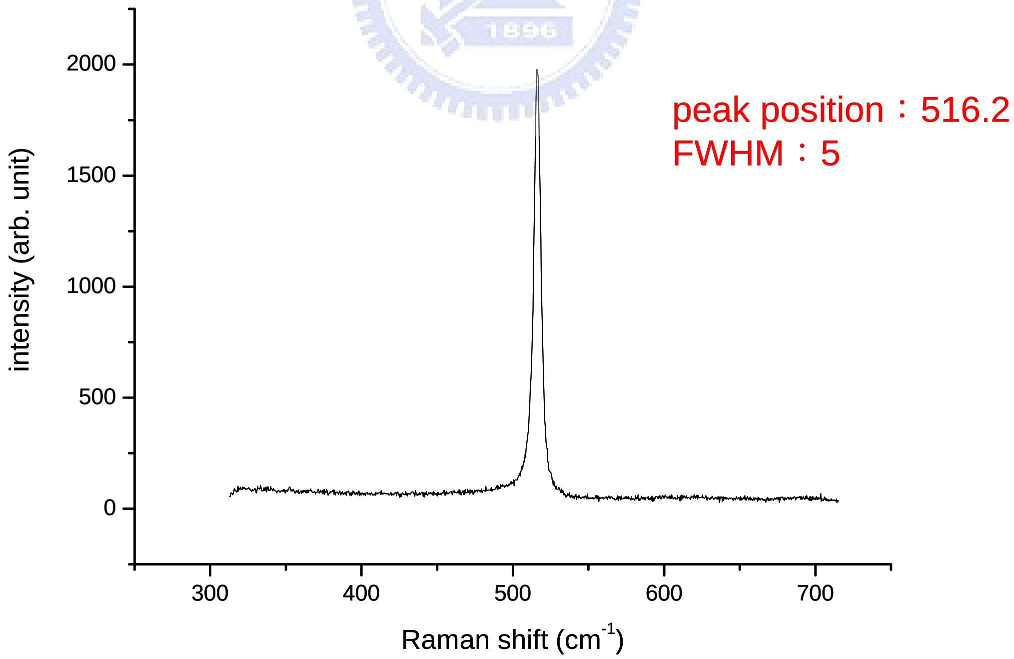

Fig.2-3-7(b) The Raman result of sample A with the laser energy density of 500*mJ/cm*^{2}

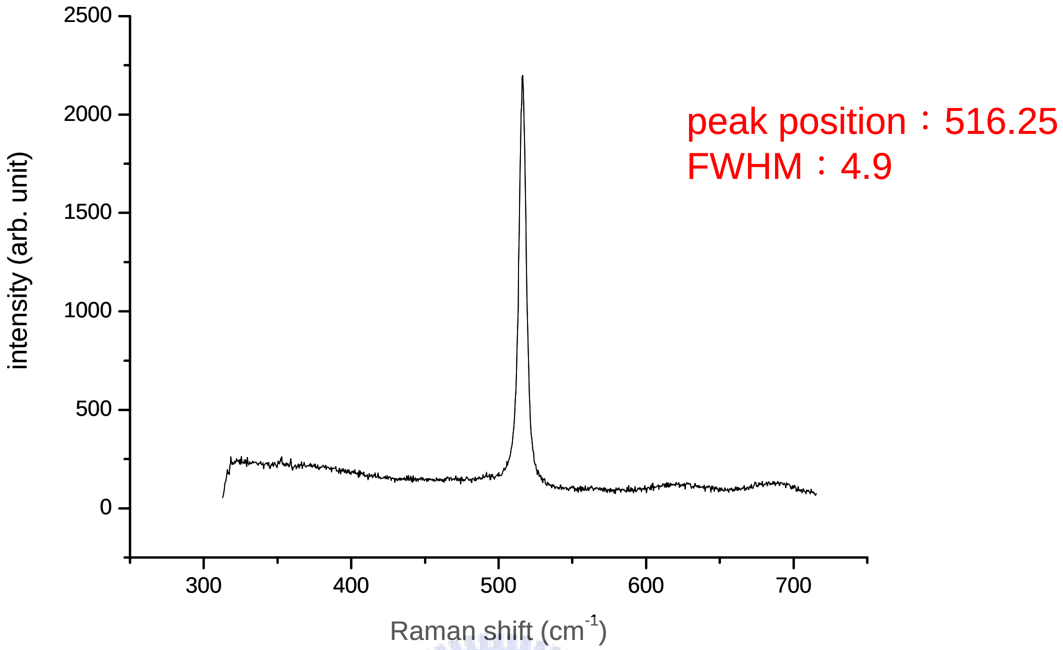

Fig.2-3-7(c) The Raman result of sample A with the laser energy density of 600mJ/cm^2

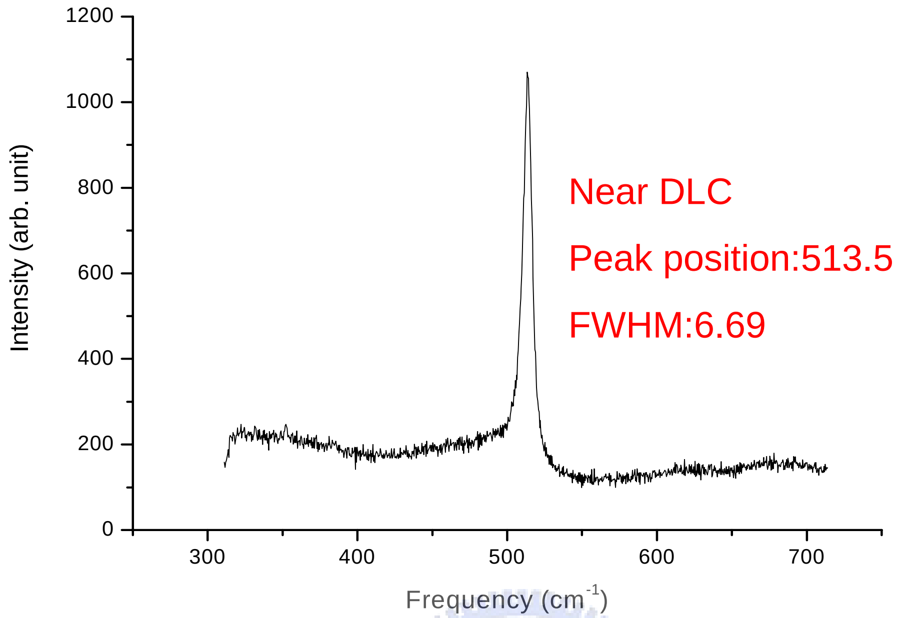

Fig.2-3-8 (a) The Raman spectra for sample B at the position of poly-silicon near DLC patterns with the laser energy density of 500*mJ/cm*^{2}

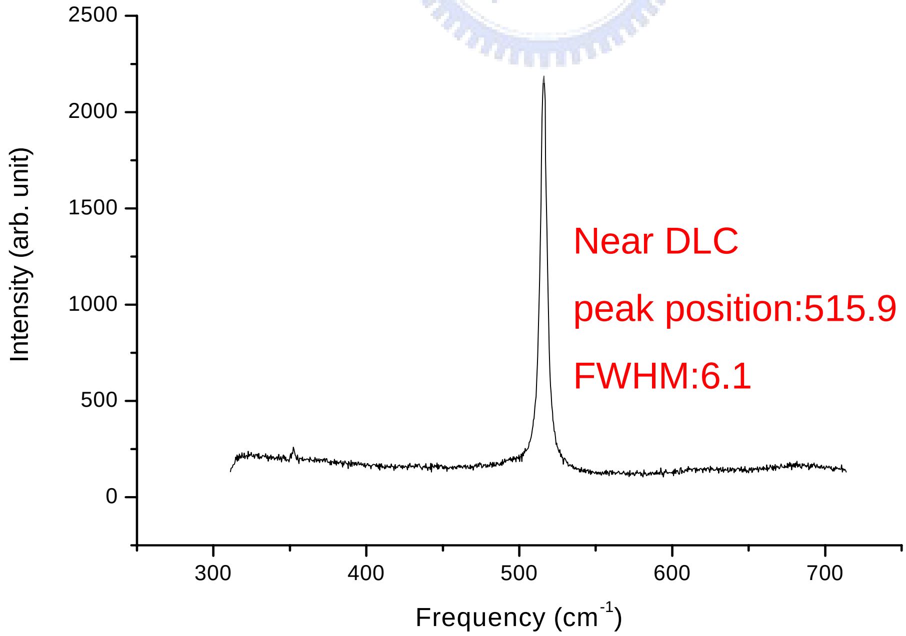

Fig.2-3-8 (b) The Raman spectra for sample B at the position of poly-silicon near DLC patterns with the laser energy density of 600*mJ/cm*^{2}

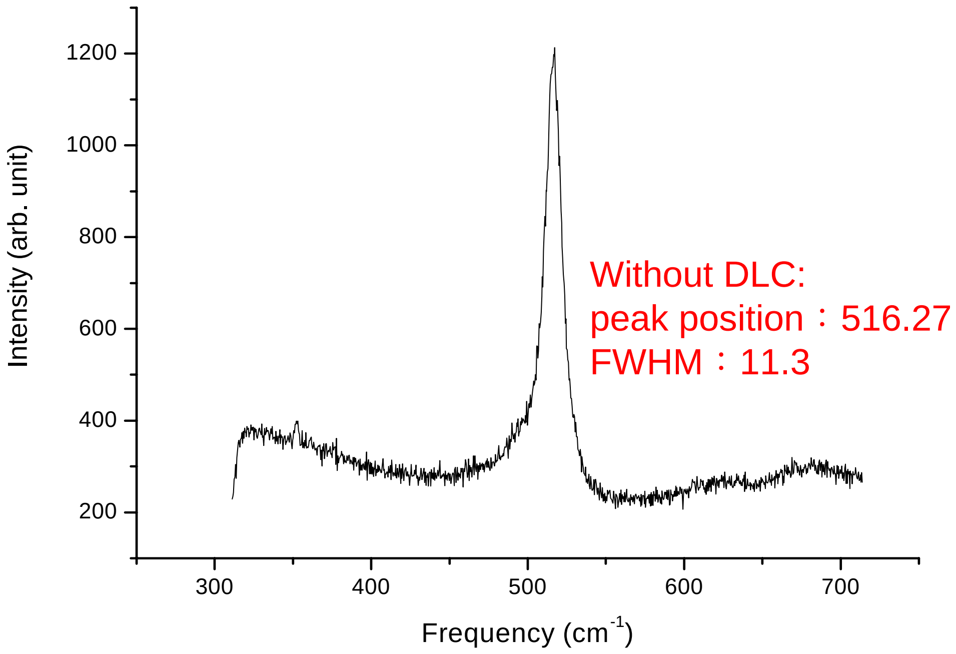

Fig.2-3-8 (c) The Raman spectra for sample C without DLC patterns

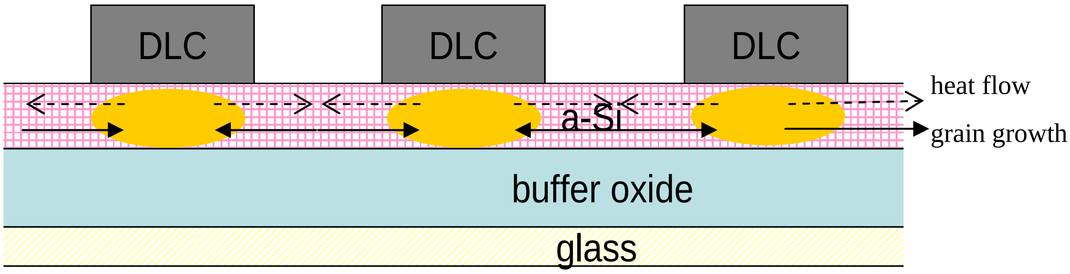

Fig.2-4-1 The schematic diagram of the proposed crystallization process

Chapter 3

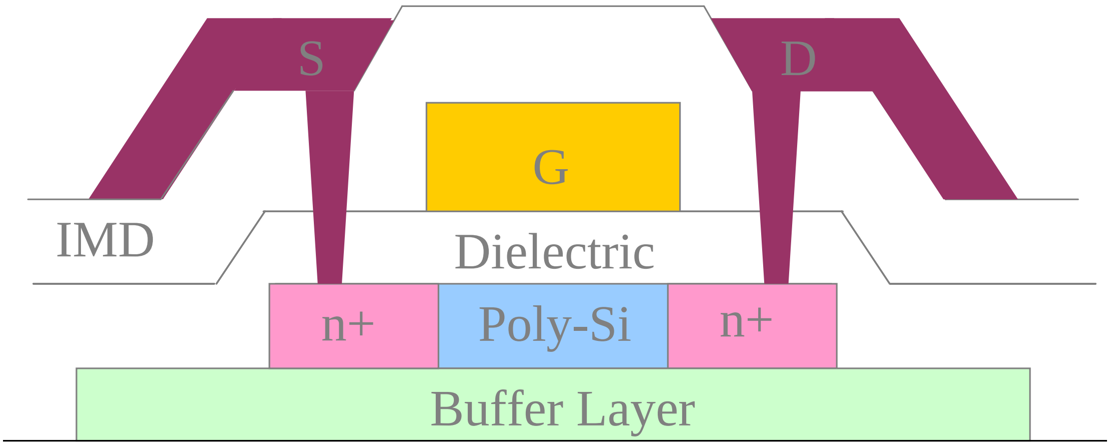

Fig.3-2-1 The cross-section of view of poly-Si TFT with self-align source/drain

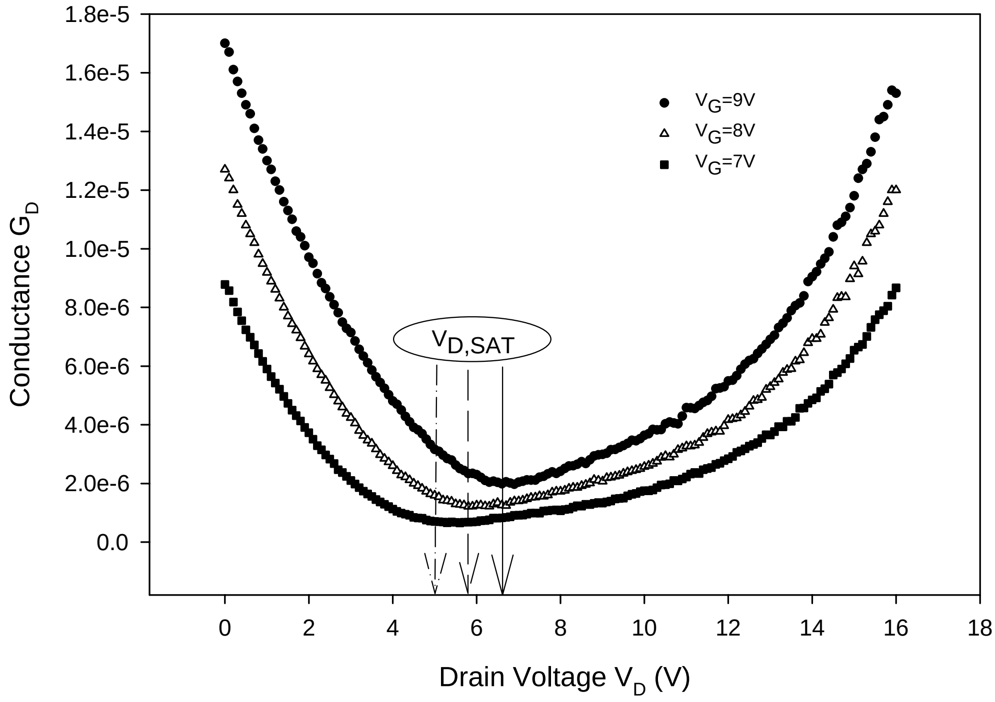

Fig.3-3-1 The saturation voltage at various gate voltages can be defined from the "first" minimum points of the conductance

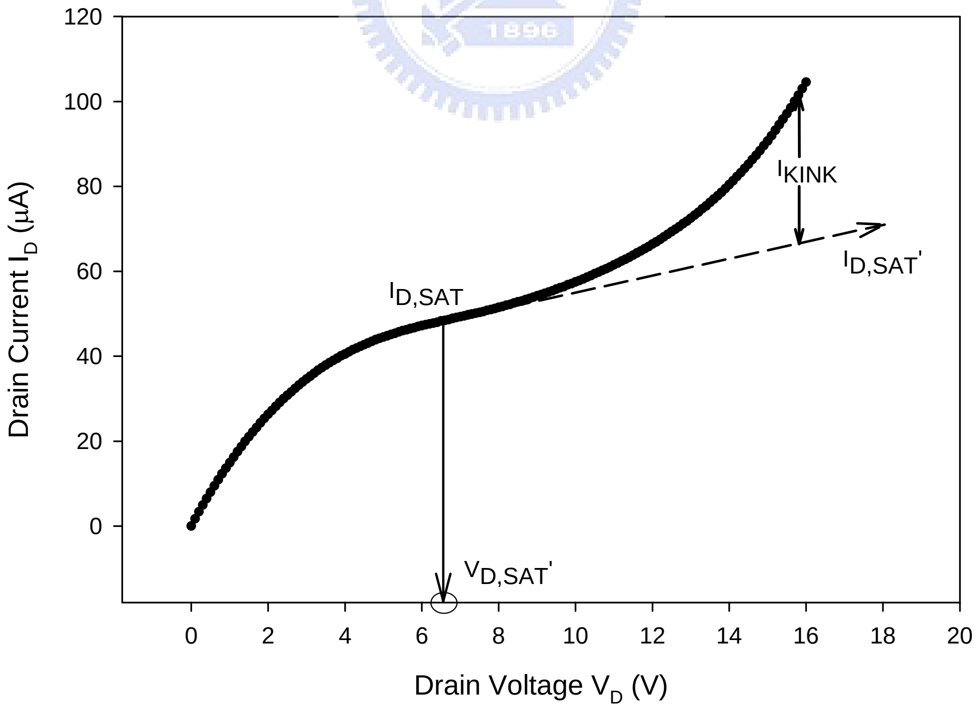

Fig.3-3-2 The kink current I_{KINK} can be evaluated by using the drain current at high drain voltage to minus the rectified saturation current, such that $I_{KINK}=I_D-I_{D,SAT}$

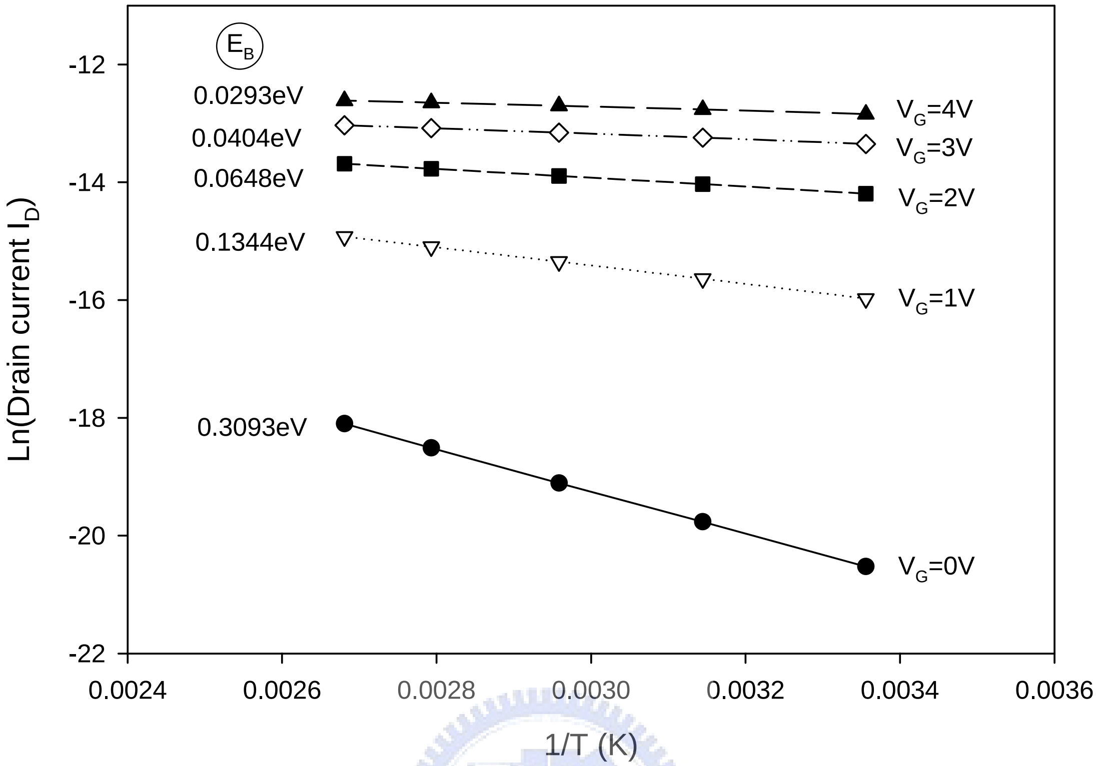

Fig.3-3-3 Arrhenius plot of the drain current of TFT with different gate voltages and $V_{DS}=0.1V$. The slope of each line defines the activation energy at the grain boundary

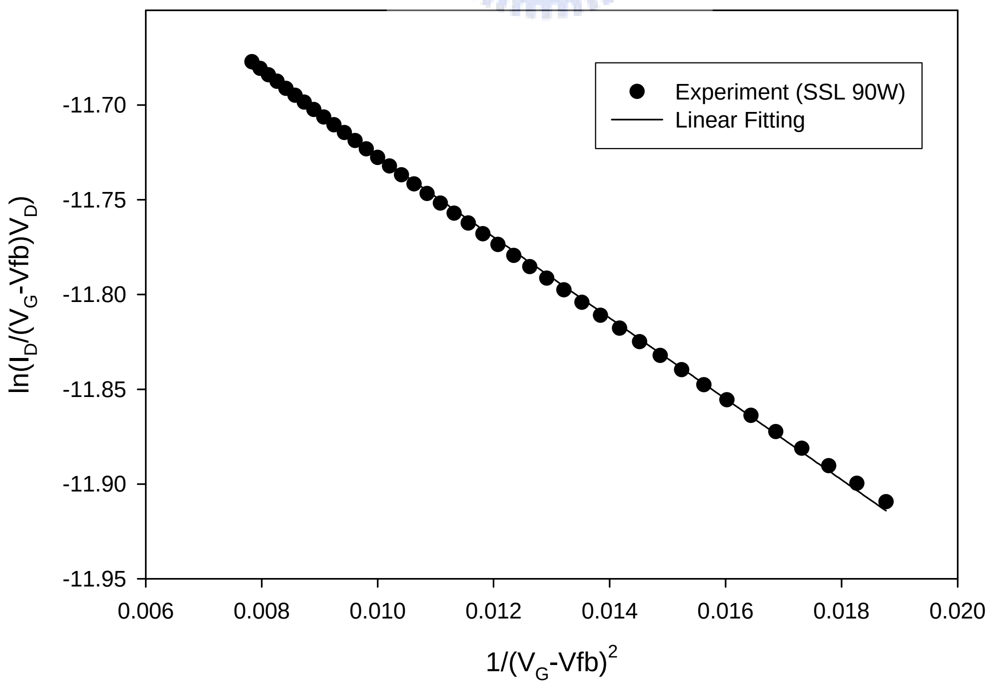

Fig 3-3-4 The trap density was extracted from slope of this plot

(a)

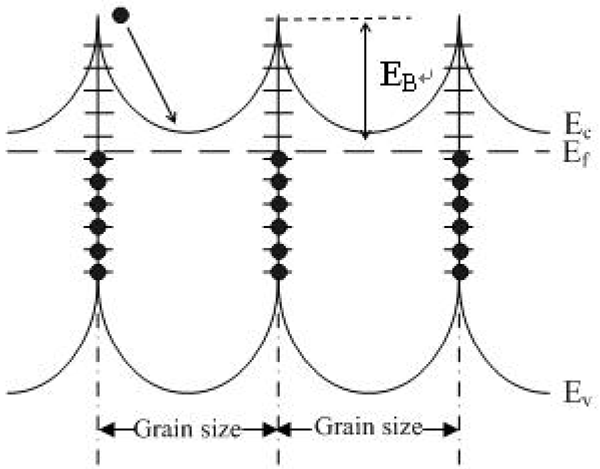

(b)

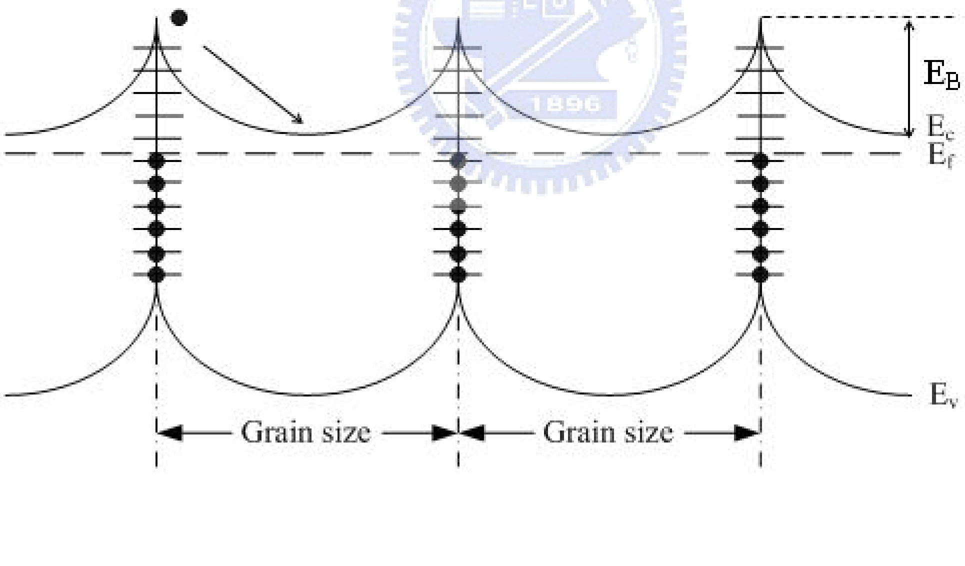

Fig.3-4-1 The model of grain boundary accelerated electron. The grain boundary barrier height is fixed. (a) carriers are accelerated by the grain boundary energy trop (b) larger grain size shows a gentler energy drop

(a)

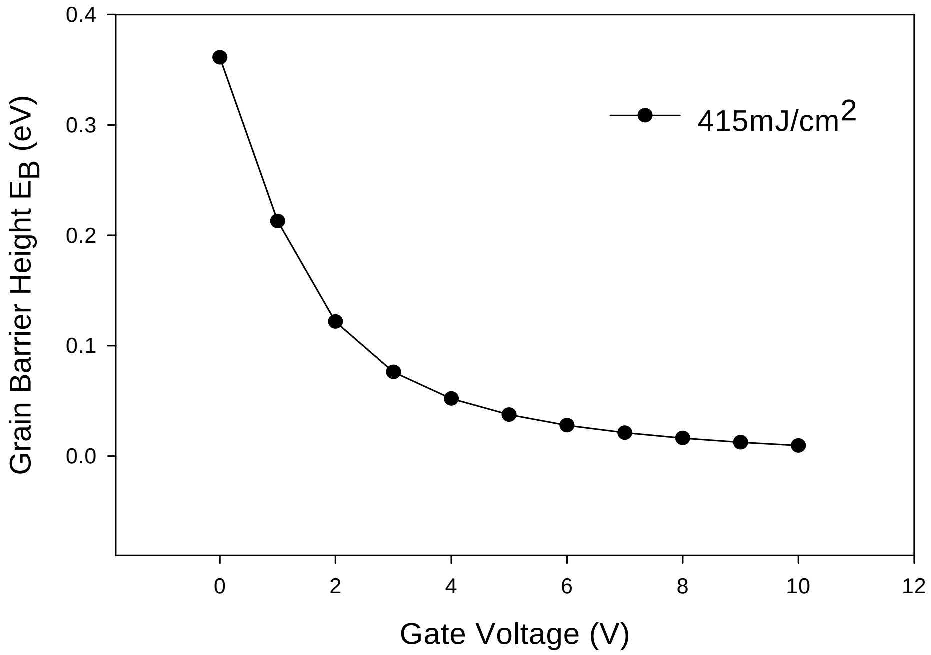

(b)

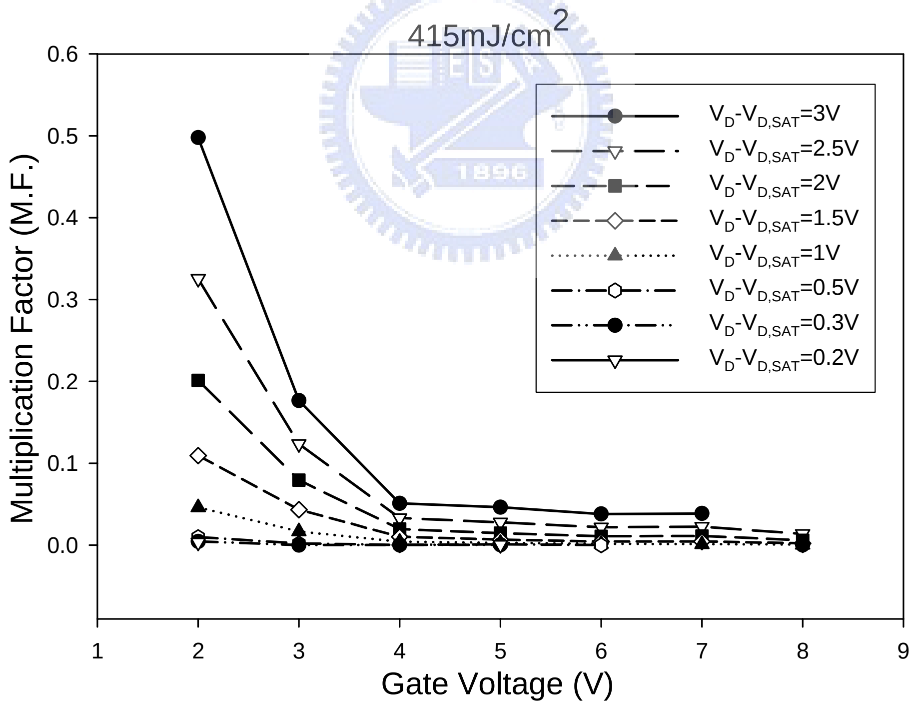

Fig.3-4-2 (a) The grain boundary barrier height with the laser energy density of 415*mJ/cm*^{2} (b) The multiplication factor with the laser energy density of 415*mJ/cm*^{2}

(a)

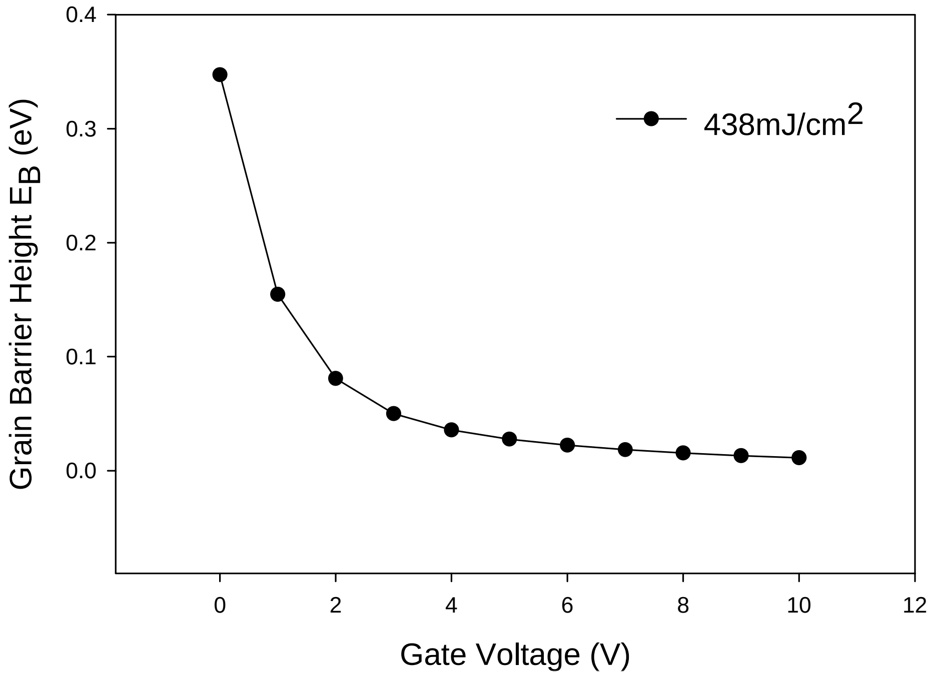

(b)

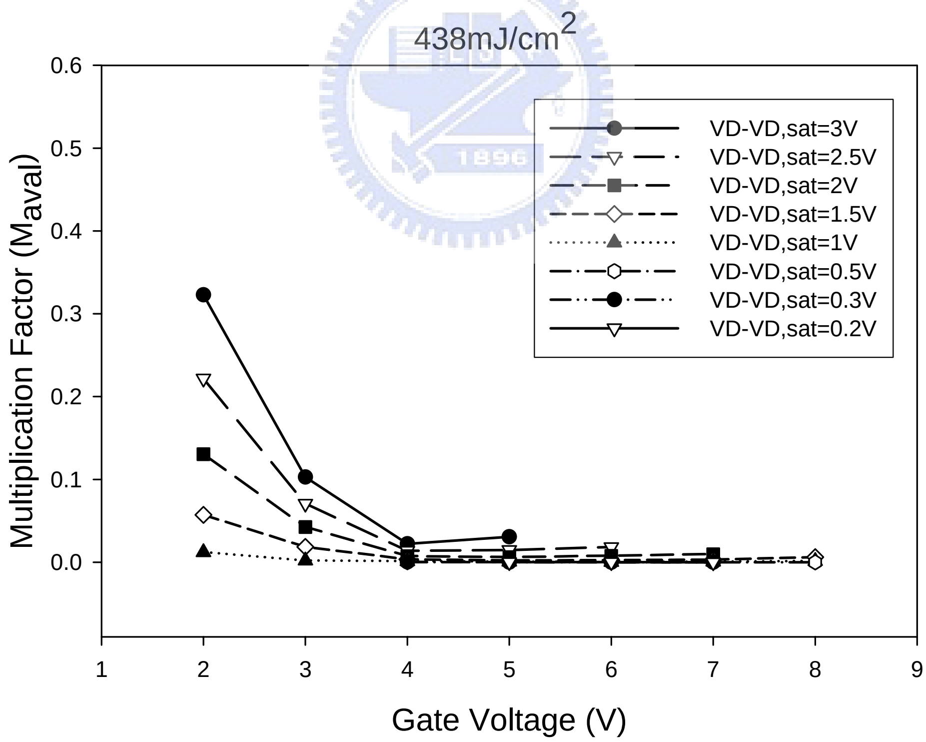

Fig.3-4-3 (a) The grain boundary barrier height with the laser energy density of 438*mJ/cm*^{2} (b) The multiplication factor with the laser energy density of 438*mJ/cm*^{2}

(a)

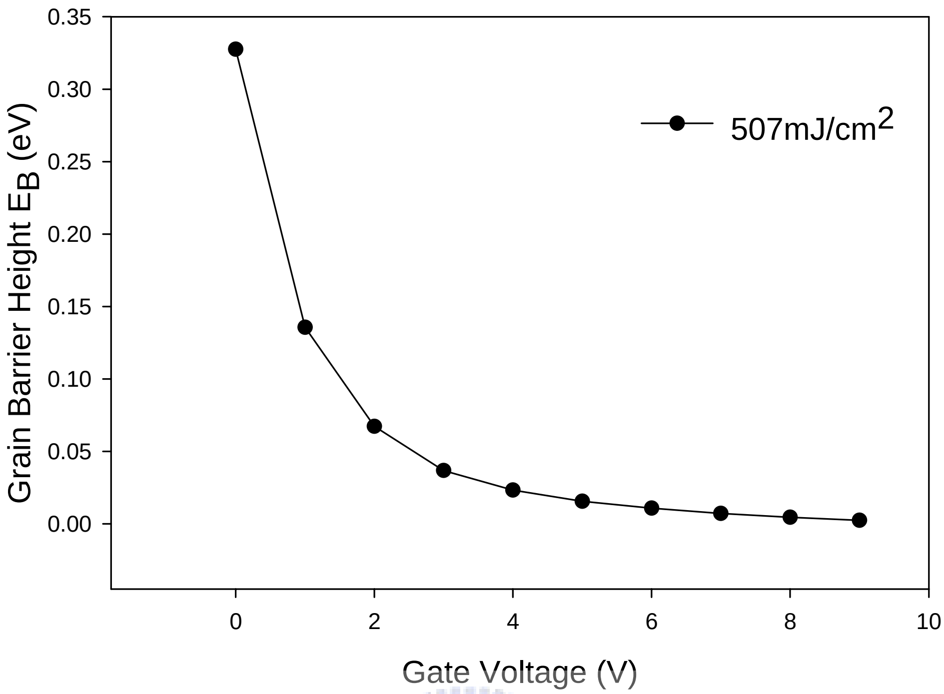

(b)

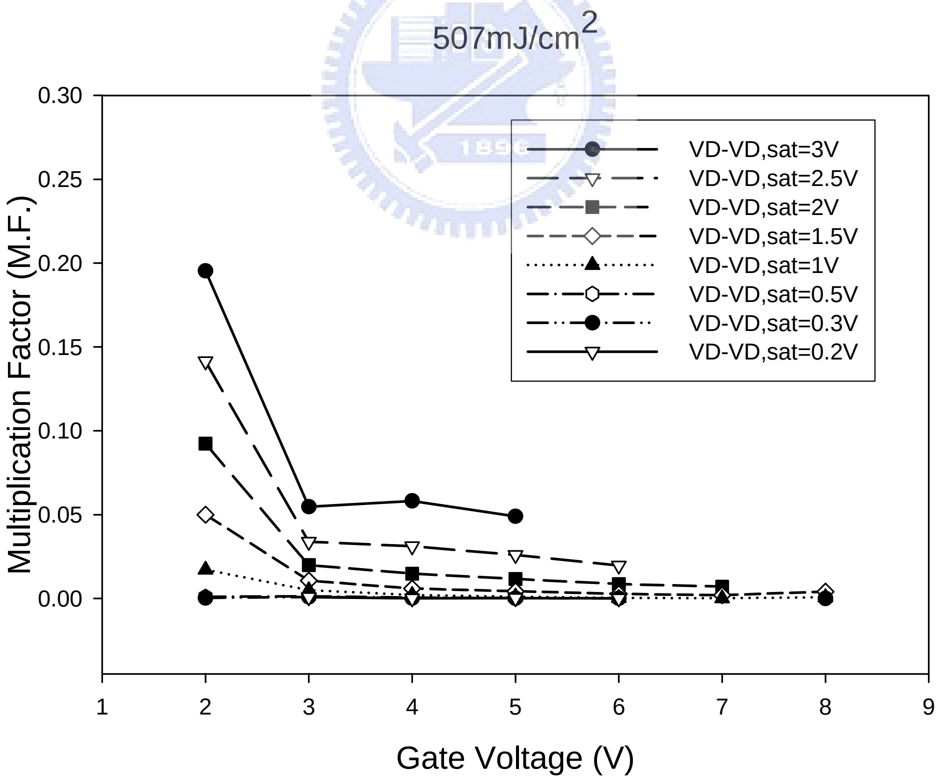

Fig.3-4-4 (a) The grain boundary barrier height with the laser energy density of 507mJ/cm^2 (b) The multiplication factor with the laser energy density of 507mJ/cm^2

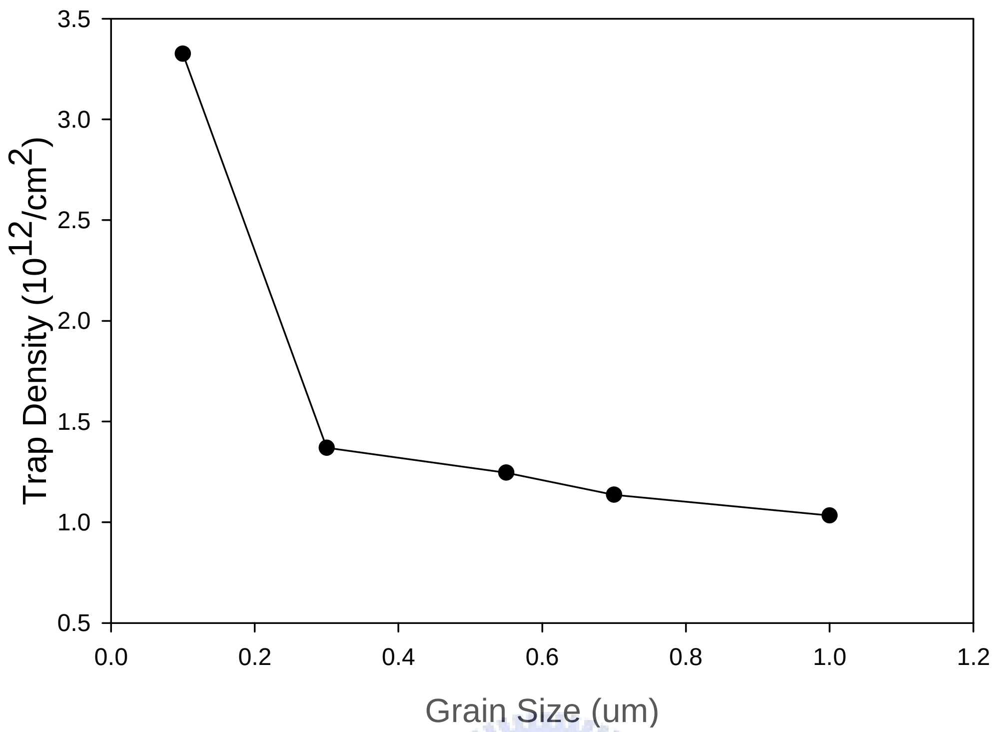

Fig.3-4-5 The trap density of SSL with different grain sizes (from 0.1*um*-1*um*)

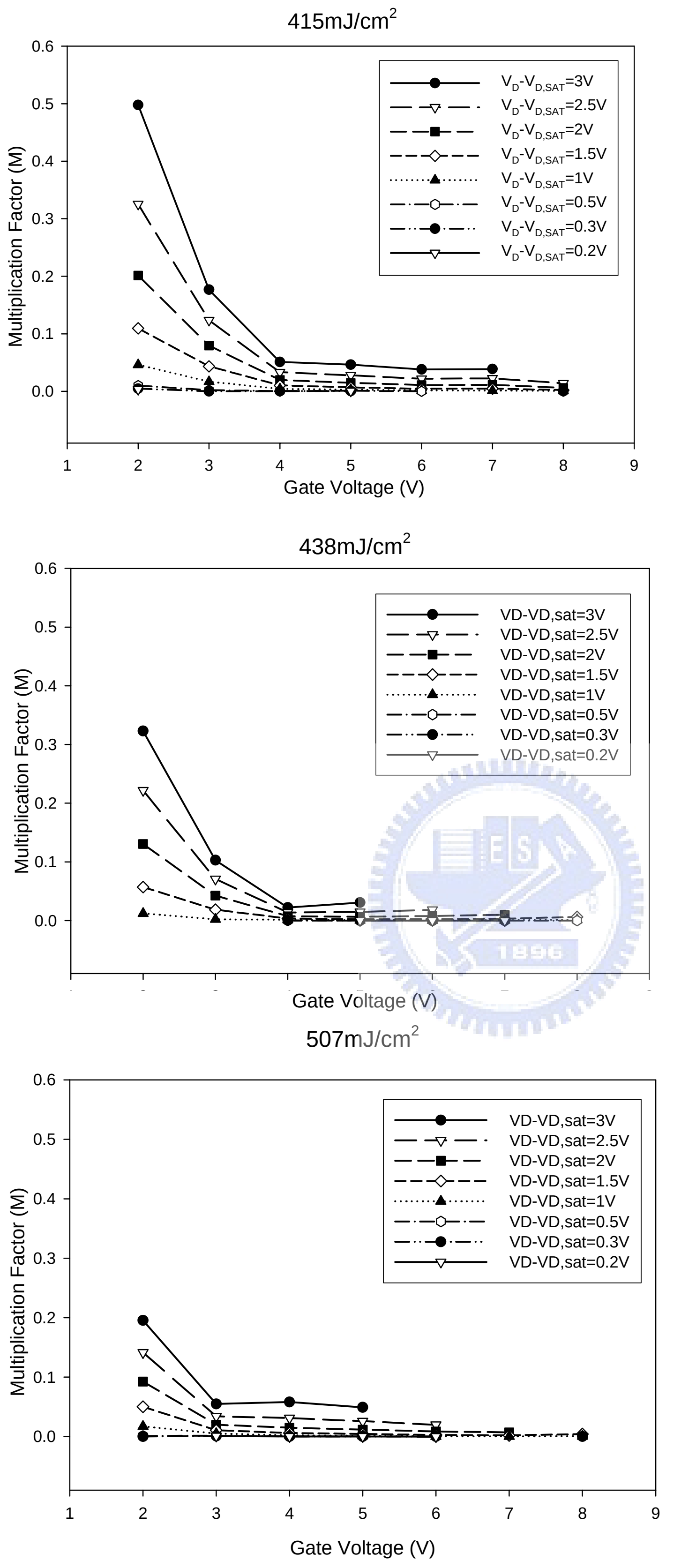

Fig.3-4-6 The multiplication factor of laser energy density form 415~507*mJ/cm²*. Multiplication factor decreases with the laser energy density increases

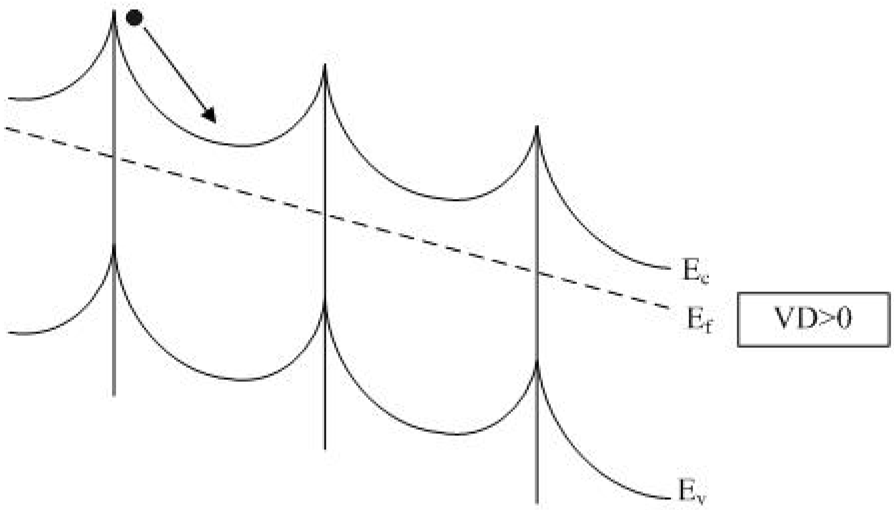

Fig.3-4-7 The band diagram of the grain boundary accelerated electron affect by the drain voltage

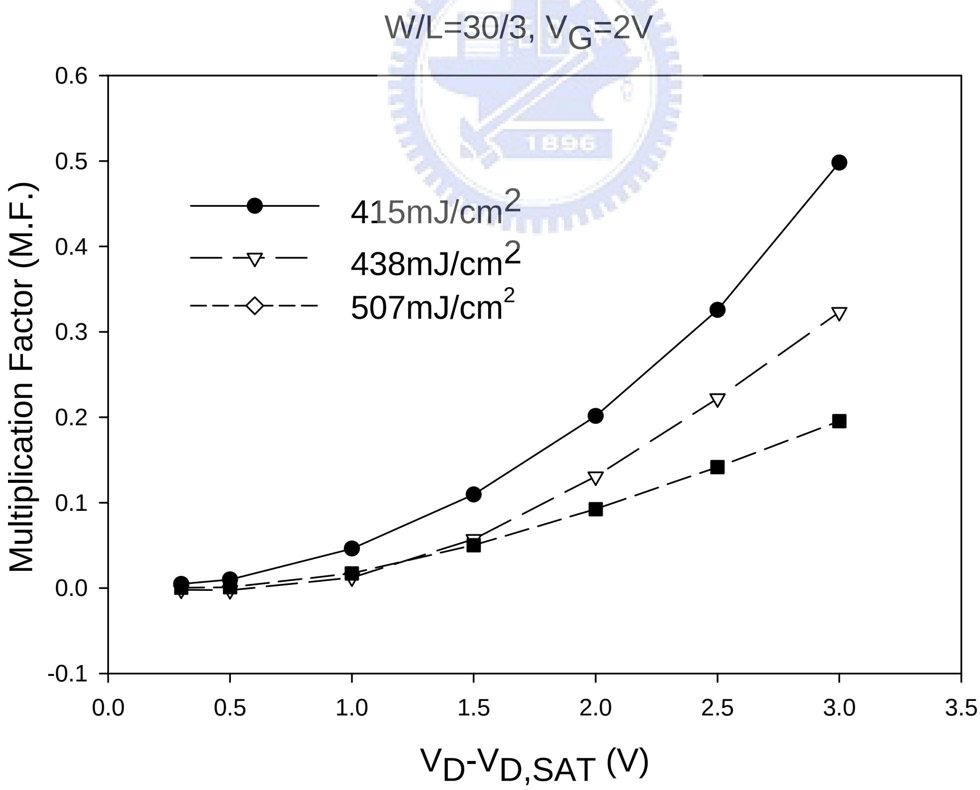

Fig 3-4-8 The multiplication factor increases with the drain voltage. And the larger laser energy density shows less serious kink effect.

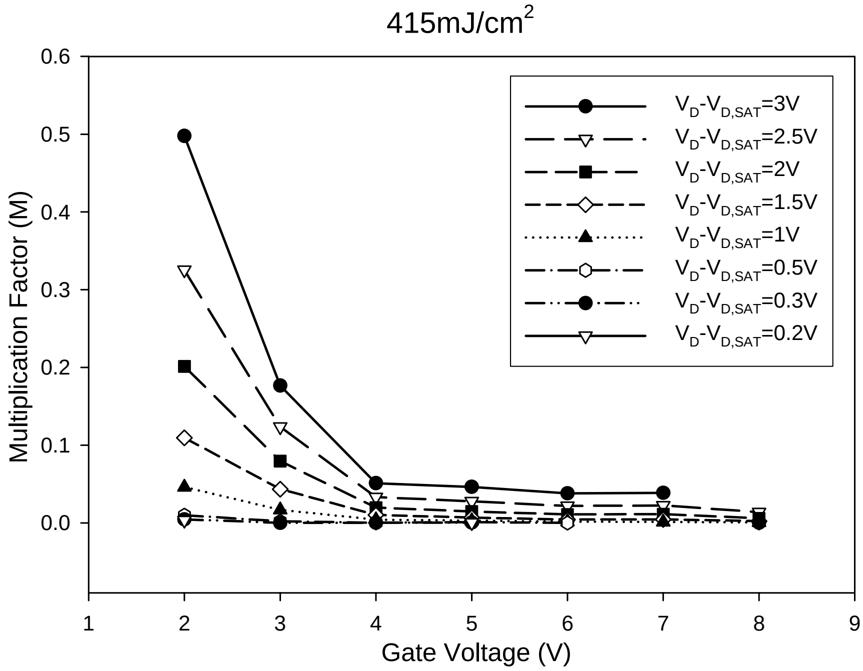

Fig.3-4-9 The multiplication factor is decreases with the gate voltage increases. Because of the effective lateral electric field lowering and the effective grain barrier height reduction

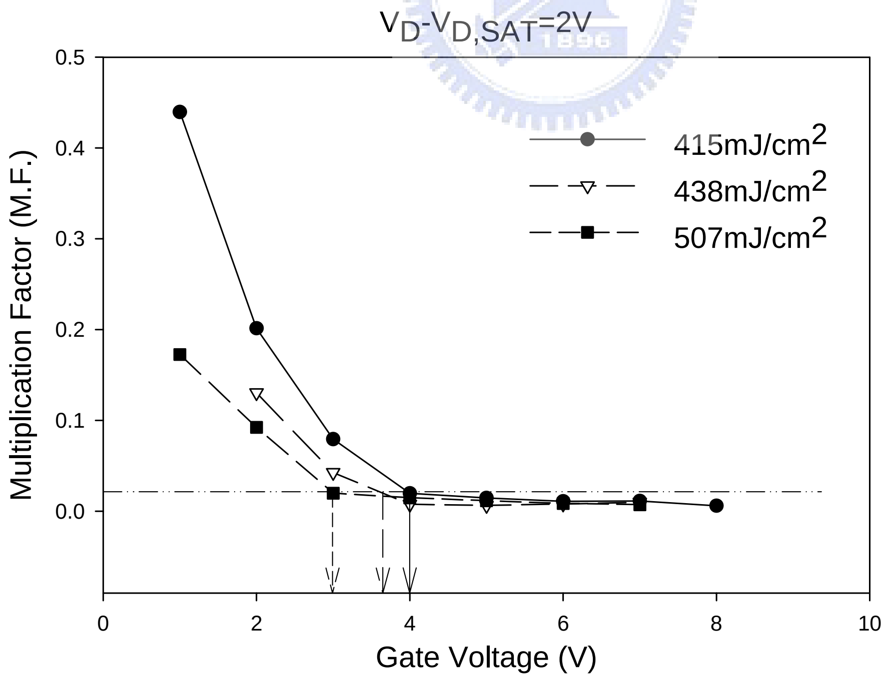

Fig.3-4-10 The multiplication factor of different laser energy density for a fixed V_D-$V_{D,SAT}$ value. The multiplication factor of a larger laser energy poly-Si film achieve a negligible small value faster

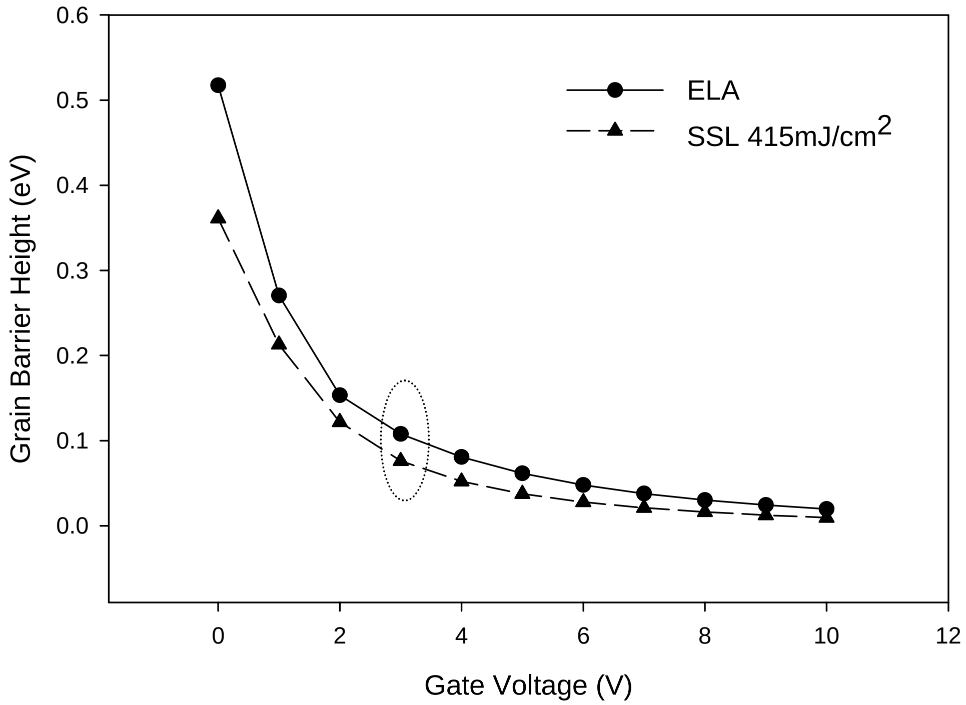

Fig.3-4-11 The grain barrier height of ELA and SSL 415*mJ/cm*^{2} silicon films. The grain barrier height of ELA is larger than the SSL 415*mJ/cm*^{2}one

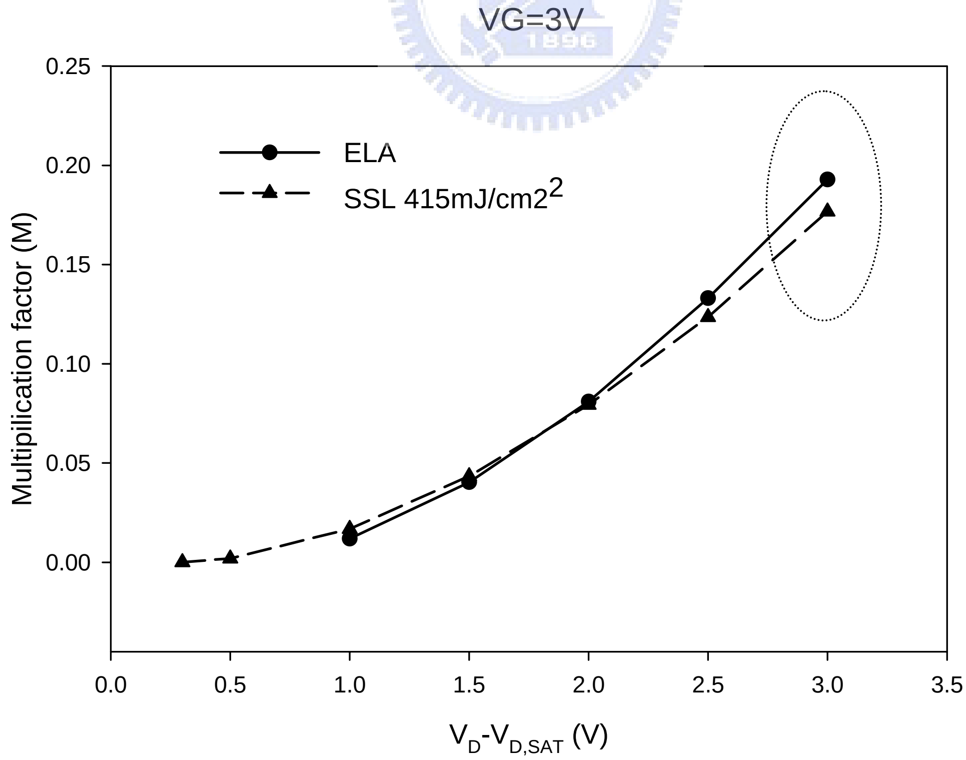

Fig.3-4-12 Under the same lateral electric field, the multiplication factor of ELA is larger than the one of SSL 415*mJ/cm*^{2}.

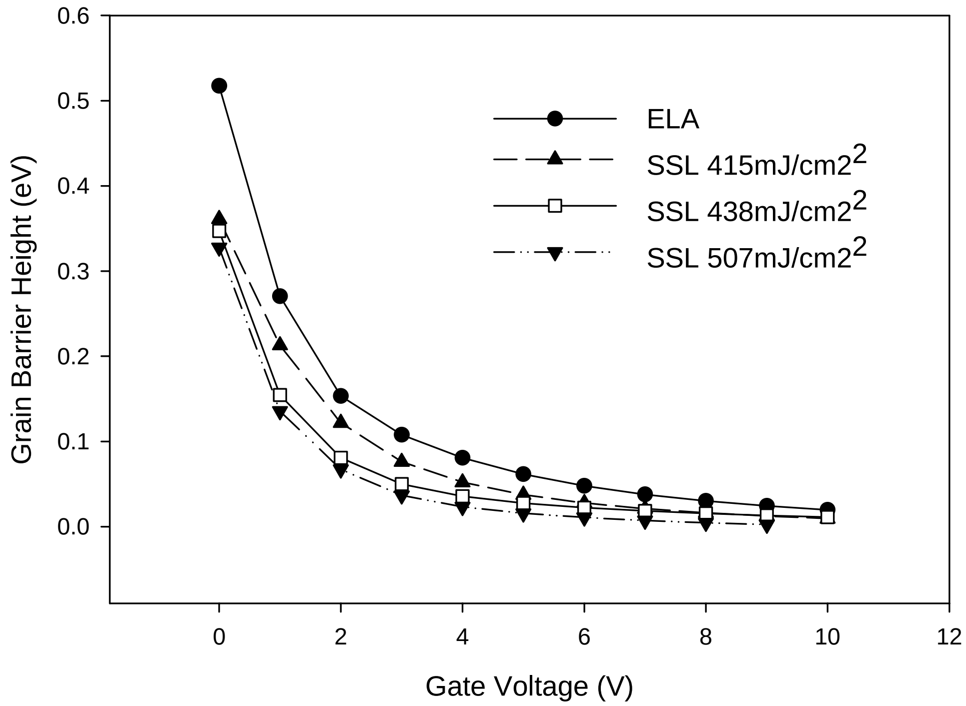

Fig.3-4-13 The grain barrier height of ELA and SSL 415~507*mJ/cm*^{2}. The grain barrier height of SSL is smaller than ELA. And also the grain sizes with laser energy density of 438*mJ/cm*^{2} and 507*mJ/cm*^{2} are much larger than ELA.

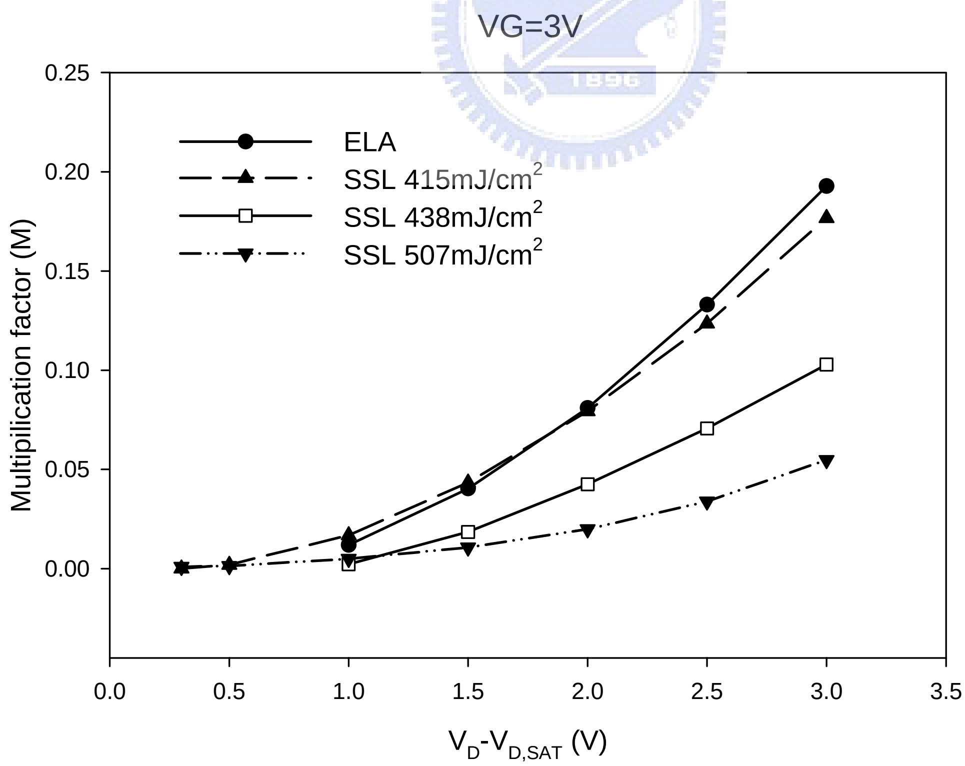

Fig.3-4-14 The grain size of SSL 438*mJ/cm*^{2} and 507*mJ/cm*^{2} is larger than ELA and the grain barrier height is also small than ELA. So the multiplication factor of SSL 438*mJ/cm*^{2} and 507*mJ/cm*^{2} is much smaller than ELA's.

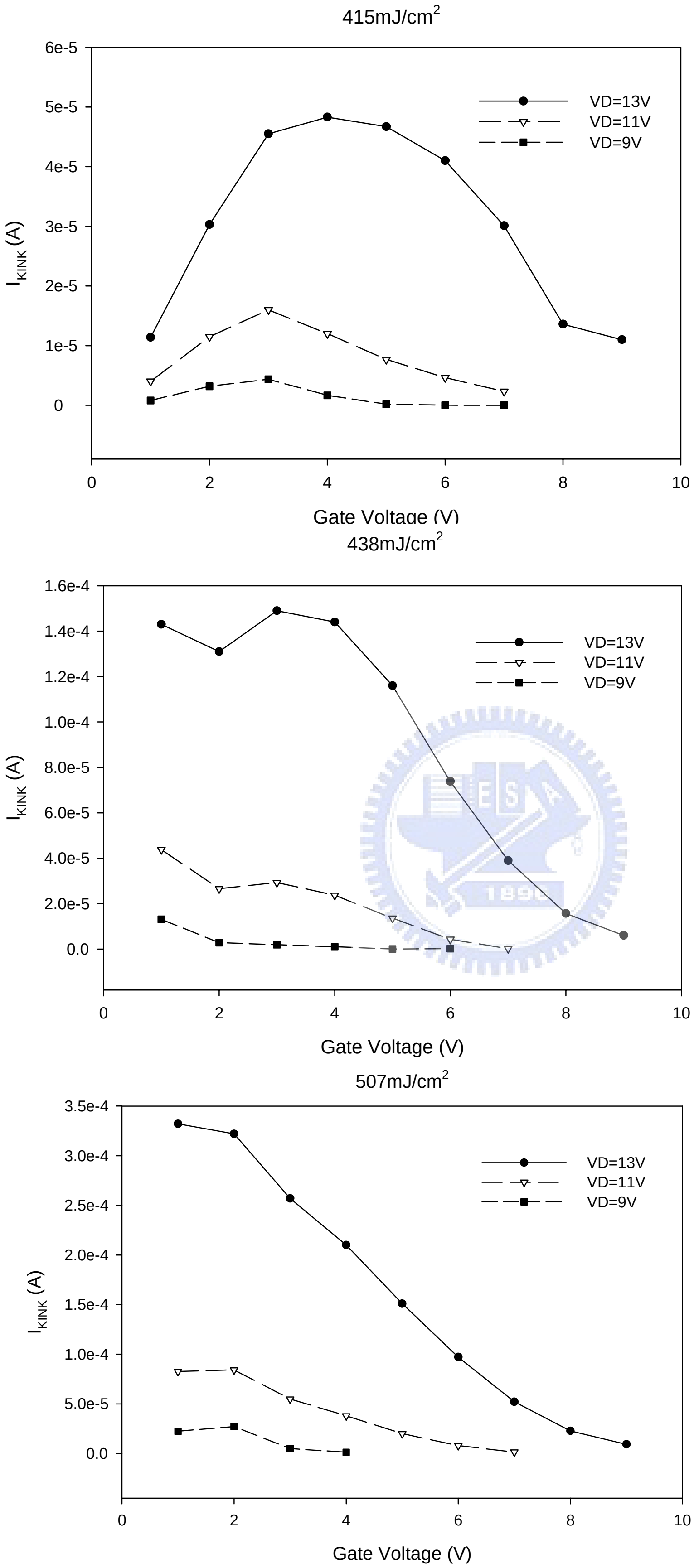

Fig.3-4-15 The kink current of SSL with laser energy density from 415*mJ/cm*^{2} to 507*mJ/cm*^{2}